Kathmandu University
Journal of Science, Engineering and Technology

Influence of heat input and shielding gas flow-rate on the microstructure and mechanical properties of dissimilar welded AA1100 and AA6070

Wasiu A. Ajibola , Stephen I. Durowaye* , Babatunde O. Bolasodun , Kehinde Nosa-Ugobor , and Oluwanifemi O. Ashaye

Department of Metallurgical and Materials Engineering, University of Lagos, Akoka, Nigeria.

Abstract

This study examined the influence of heat input and shielding gas flow-rate on the microstructure and mechanical properties of V-joint welded aluminium alloys of 1100 and 6070 plates. The as-received AA6070 was an off-cut billet and was cast into a flat plate of 5 mm using the green sand moulding technique. AA1100 was used in the as-received condition. Plates of dimension 50 x 50 x 5 mm were prepared for the Tungsten Inert Gas (TIG) welding with heat input ranged between 52.5 J/mm and 69.1 J/mm and shielding gas (argon) flow rate of 7 and 13 L/min. The visual inspection indicated that welds were free common defects with no distortion. The results obtained from the experiments showed that the predominant phases in the microstructure of the samples were $\alpha - Al$, $AlSiO_2$ and $AlFeSiO_2$, which characterised the strengthening mechanism of the weld joints. At a current of 70 A, and shielding gas flow rate of 7 L/min, the microstructure showed more of dendritic structure, which mainly contained $\alpha - Al$ and $AlSiO_2$. When the gas flow rate increased to 10 L/min, the dendritic structure broke into platelets with no oxygen gas diffusion. The weld joint demonstrated the highest hardness value of 72 HV at 70 A and 13 L/min gas flow rate. The weld joint demonstrated the highest ultimate tensile strength of 86 MPa at 130 A and 10 L/min.

Keywords: Aluminium alloy; Heat input; Gas flow-rate; TIG welding; Mechanical properties.

1. Introduction

Aluminium has a desirable combination of properties such as low density, adequate strength, and production processes that are not complex, which can be modified by alloying. Aluminium alloys are classified as non-heat-treatable and heat-treatable alloys. The first group includes pure aluminium alloys (series 1xxx) and alloys with the primary alloying element: manganese (3xxx series), silicon (4xxx series), and magnesium (5xxx series). The second group consists of aluminium alloys with the main additives: copper (2xxx series), magnesium and silicon (6xxx series), and zinc (7xxx series) [1].

Aluminium alloys have attracted a lot of interest or attention in industries like aerospace, shipbuilding and automotive due to the possibility of combining different alloys in one structure. Joining dissimilar materials is challenging but essential for many applications as the advantages of different materials can be well-exerted [1]. Because of the importance of making joints of aluminium alloys, developing an economically suitable welding method and optimizing the welding parameters are considered a challenge for expanding its industrial applications. However, fusion-welding processes are the most common technique for joining metal alloys [2, 3].

The two main fusion-welding processes used in joining process are tungsten inert gas (TIG) and metal inert gas (MIG). The TIG welding process involves the formation of an electric arc between the non-consumable tungsten electrode and the welding plates. This arc provides sufficient energy to melt the welding plates in the weld zone and the filler metal [4, 5, 6]. The MIG welding process generates a constant electric arc between an automatically fed consumable electrode and a joint plate in the weld zone with an inert gas shield [7]. Welding represents a lasting joining technique wherein heat and/or pressure is applied to unite diverse ferrous and nonferrous materials, including metals and alloys, at their points of contact. This method is widely employed, particularly in aluminium welding, where alloys are liquefied at the interface to fuse work-pieces, resulting in a durable joint upon solidification [8].

Welding is the favoured amalgamation method for most structural engineering applications [3]. To enhance bonding strength, a filler material is introduced, creating a molten weld pool that solidifies to form a robust connection between the materials. The performance of welded materials is contingent upon factors such as the metal's melting point, thermal conductivity, reactivity, thermal expansion, electrical resistance, and surface conditions [8]. Among the types of welding, Tungsten Inert Gas (TIG) welding is unique and stands out as an arc welding method employing a tungsten electrode, which remains non-consumable. The electrode is linked to a vital power source, and a shielding gas, typically argon or helium, is often utilized to safeguard the welding surface from the atmosphere. The addition of filler metal is optional and depends on the specific weld type [8].

Conditioning welding is particularly valuable for joining challenging materials like aluminium and magnesium and TIG welding ensures high-quality weld, which is achieved through the heat coalescence that is generated by an electric arc between the non-consumable tungsten electrode and the metal. Throughout the process, gases are created by heating the work-piece and filler pin to facilitate welding. Helium and argon serve as shielding gases due to their non-reactive nature. These inert gases shield the weld-

*Corresponding author. Email: sdurowaye@unilag.edu.ng

ing area, preventing dust, minimizing oxidation, facilitating heat transfer during welding, and aiding in the initiation and maintenance of a stable arc, thanks to their low ionization potential [8].

TIG welding has remarkable flexibility but mastering it can be challenging because it requires the use of two hands. One hand feeds the rod, while the other handles the TIG torch that is responsible for generating the required heat and arc. This torch is versatile enough to weld a variety of conventional metals, including copper, steel, nickel alloys, cobalt, and titanium alloys [8]. The TIG welding is a method of electro-arc welding that generates the fusion energy via an electric arc burning between the work piece and the electrode. The electrode, arc, and solder pool are shielded by an inert gas during the welding cycle against the harmful effects of ambient air. The gas shielding through the gas nozzle leads to the soldering area, where the ambient air substitutes. TIG welding varies in the sense that electrodes are not consumed unlike other arc welding methods [8].

The tungsten and the welding zone are protected from the surrounding air by a gas shield (inert gas). The electric arc can produce temperatures of up to 19,400 0C and this heat can be much focused local heat [5].

The TIG welding process is so good that it is widely used in the high-tech industry applications such as, nuclear industry, aircraft, food industry, maintenance and repair work and some manufacturing areas [5]. Studies [1,2, 3, 8, 9] have been conducted on investigating the mechanical properties of weldments adopting various welding parameters and the results indicated improved properties. Because of the importance of aluminium alloys and welding in engineering, this study is undertaken to evaluate the influence of heat input and shielding gas flow-rate on the microstructure and mechanical properties of dissimilar welded AA1100 and AA6070.

2. Methodology

2.1. Materials and equipment

The followings are the materials used for this study: Aluminium Alloy 6070 (AA6070), Aluminium Alloy 1100 (AA1100), Tungsten non-consumable electrode (Ø1.60 mm), Argon (Ar) gas 99.98 % pure, distilled water, aluminium filler metal ER 4043 (∅2.40 mm) and sand mould. The AA6070 was obtained from Tower Aluminium Nigeria Limited, Sango Ota, Ogun State, Nigeria. The AA1100 and filler wire ER4043 was sourced from local vendors in Lagos State, Nigeria. To confirm the nominal chemical compositions of these materials, X-ray Fluorescence spectrometric analysis (Model: Spectomax LM806-Amatek, USA) was conducted. Tables 1 and Table 2 show the nominal chemical compositions of the AA6070 and AA1100. Table 3 shows the nominal chemical composition of filler wire 4043. It is important to mention that the filler wire was selected because of its proximity in terms chemical composition to AA6070.

The equipment used during the course of this study: MET 400 DCi ERGUS GTA welding machine, Universal tensile machine (SATEC 600DX, K9360, 600KN capacity), hacksaw, moulding pattern, MMT-X7A micro hardness tester HV5, weighing balance, impact test machine, scanning electron microscope (Model: JSM 7600F), grinding and cutting machine, measuring tape, spectrometer analyser.

2.2. Samples preparation

A typical TIG welding station setup and principle are shown in Fig. 1 and Fig. 2. The as-received AA6070 is an off-cut billet. Hence, hacksaw was used to cut the billet into smaller sizes and subsequently cast into a flat sheet of 5 mm thick using the green sand mould technique. The use of a green sand mould for casting AA6070 may introduce porosity or inclusions that alter welding outcomes, which could be a limitation. The casting technique include; pattern making, moulding of pattern, charging of the AA6070 into pit furnace, shakeout of the cast and felting of cast. Fig. 3 shows the samples in the pit furnace and samples preparation. The AA1100 was used in the as-received condition. AA1100 and AA6070 samples were cut into dimension 50 x 50 x 5 mm. To ensure consistent root gaps of 2.40 mm, the dissimilar plates were first tack welded (Fig. 3c) prior to proper welding operation. For all the experimental set-up of the joining procedure, single V notch butt joint configuration was prepared. Fig. 4a, Fig. 4b, Fig. 4c show the schematic diagram, prepared samples, and one of the as-welded samples of the joints produced respectively. Visual inspection of the welded sample gives first impression about the quality of the welded joints. There was no visible presence of defects such as undercut, overlap, surface cracking, surface porosity, under fill or incomplete root penetration. The welded samples were free from any form of defect with characteristics of continuous tracks seen. Furthermore, there was no evidence of spatters generated during welding process with various combination of welding parameters and varied gas flow used. This suggests that a stable arc condition was achieved.

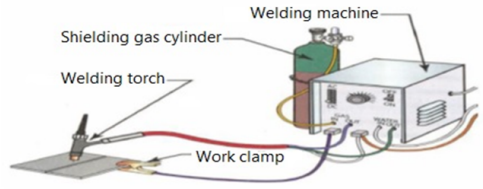

Figure 1: TIG welding station setup [5].

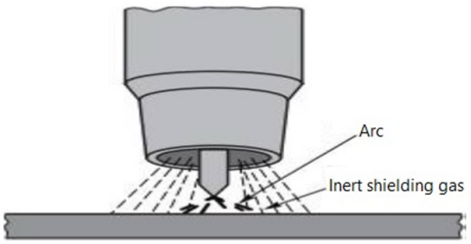

Figure 2: TIG welding principle [8].

2.3. Welding procedure

To investigate the influence of heat and gas flow rate on the weld profile of welded AA6070 and AA1100, a TIG welding machine (Model: ERGUS MET 400 CDI) was used. Table 4 shows the selected welding parameters used to obtain the applied heat input. Other welding parameters such as type of welding electrodes, arc length, torch angle, diameter of the electrodes, tolerance, and type of shielding gas were not varied in this study. This is to allow for the evaluation of effect of heat input and gas flow rate. Equation 1 [10] was adopted for the calculation of the heat input.

$$Heat\ Input\ (HI) = \frac{Current\ (A) * Voltage\ (V) * 0.06}{Travel\ Speed\ (v)} \quad (1)$$

Where: HI is in KJ/mm, arc voltage is in volts (V), and travel speed (v) is in mm/min.

The tungsten electrode of 1.6 mm in diameter was initially ground to give a pointed tip, as pointed tip allows the welding current to transfer in a focused arc and helps prevent thin metals (such as aluminium) from becoming distorted and pure argon

Table 1: Nominal chemical composition of AA6070 (part A).

Al	Si	Fe	Mg	Zn	Cu	Mn	Ni	Sn	V	Pb	Ti
96.720	1.250	1.060	0.370	0.218	0.188	0.091	0.034	0.024	0.023	0.0186	-

Table 2: Nominal chemical composition of AA1100 (part B).

Al	Si	Fe	Mg	Zn	Cu	Mn	Ni	Sn	V	Pb	Ti
99.370	0.340	0.240	_	0.0071	_	_	0.0056	_	0.0240	0.0009	0.0140

Table 3: Nominal chemical composition of filler wire ER4043.

Al	Si	Fe	Be	Cu	Mg	Mn	Ti	Zn
Bal	4.5 6.0	0.8 max	0.0008 max	0.30 max	0.05 max	0.05 max	0.20 max	0.10 max

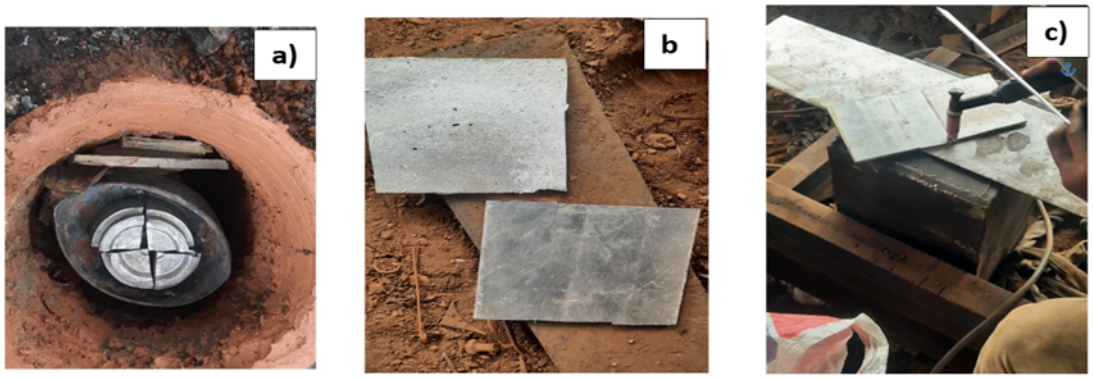

Figure 3: (a) Samples melting in the pit furnace. (b, c) Samples preparation.

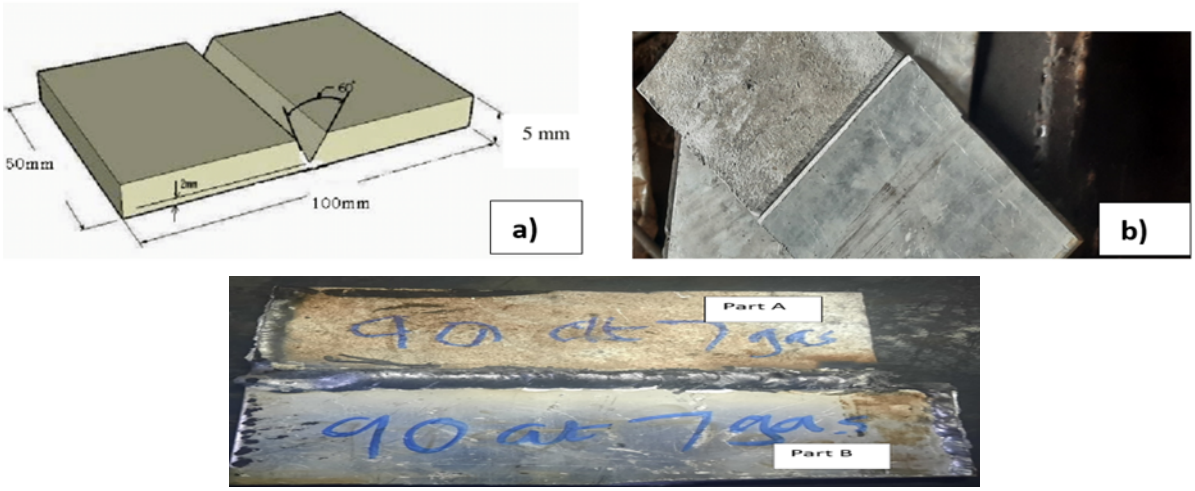

Figure 4: (a) Schematic diagram of samples. (b) Prepared samples. (c) One of the as-welded samples of the joints.

was used as shielding gas. The current used was varied from 70 - 130 A and the gas rate used were 7 l/min, 10 l/min and 13 l/min, while a constant voltage of 240 V was used for all welding processes. To eliminate contaminants prior to welding, acetone solution of 2 % Nital was used to clean the surfaces of the prepared plates. The samples were clamped on a bench to reduce distortion during welding. Thereafter, welding operation was conducted at room temperature.

2.4. Microscopy and mechanical testing of samples

2.4.1. Microstructural examination

To gain insight into the dissimilar aluminium alloys welded joint, metallographic analysis was performed. The microstructure of the dissimilar welded aluminium alloys substrates were observed with the aid of JSM 7600F – Schottky Field Emission Scanning Electron Microscope. A microstructural test-sample of 40 x 40 mm was cut from each of the welded samples. The sequence of sample preparations for metallographic examination used are grinding, polishing and etching. The grinding was performed with silicon carbide grit paper with the range of 80, 200, 600 and 1200 microns. Good surface finishing was obtained with 1 µm colloidal silica. Finally, a mirror like surface was achieved with aid of solutions of phosphoric acid, nitric acid, acetic acid and water, according to ASTM E407, which was adopted by [11].

2.4.2. X-ray diffraction (XRD) test

The phases present in the welded joint of the dissimilar aluminium alloys were identified using an X-ray diffractometer (XRD). The welded areas were irradiated with the incident X-rays and the intensities and scattering analysis to evaluate phases present according to ASTM E3-11.

2.4.3. Hardness test

In accordance with ASTM E384 standards, the hardness test of the dissimilar welded aluminium alloys was conducted by using a Vickers hardness MMT – X75 micro hardness tester HV5. In each of the weld bead zone, parent materials and heat-affected zone, three indentations were obtained. Each test took 10 seconds under a load of 980.66 mN.

2.4.4. Tensile test

The tensile test samples were prepared from the dissimilar welded aluminium alloys. All the welded samples were prepared using a milling machine. The tensile test was conducted on the tensile testing machine SATEC 600Dx, K9360, 600 KN according to ASTM E8/E8M standards. During the test, the samples suffered fractured and the generated data form the machines in form of load and extension were converted to stress – strain for the interpretation.

3. Results and discussion

3.1. Microstructure

During welding of dissimilar aluminium alloys when using a filler wire, materials in the fusion zone experience temperature above 800^oC with a transformation within the aluminium alloys. The microstructure reveal the presence of $\alpha - Al$, SiO_2, $AlFeSiO_2$, and $AlSiO_2$ phases in the weld joint (fusion zone), which are influenced by the applied heat input and gas flow rate. Fig. 6 shows the scanning electron microscope results of weld zone for the welded samples at current of 70, 90, 110, and 130 A at shielding gas flow rates of 7 and 10 L/min. The figure generally shows the orientation, distribution and volume fraction of the phases present. At a current of 70 A, and shielding gas flow rate of 7 L/min, the microstructure shows more of dendritic structure, which mainly consists of $\alpha - Al$ and $AlSiO_2$. However, when the gas flow rate was increased to 10 L/min, the dendritic structure broke into platelets with no oxygen gas diffusion. At a lower current of 70 A, there was more precipitation of Fe in the matrix of the $\alpha - Al$. The SEM result of sample produced with current of 90 A is shown in Fig. 6c, the presence of grain boundaries are well visible. Predominant phases in terms of volume fraction and distribution in Fig. 6c, Fig. e and Fig. g are $\alpha - Al$, $AlFeSiO_2$, and $AlSiO_2$ when the shielding gas flow rate was 7 L/min. Further increase in shielding gas flow rate to 10 L/min reduced the presence of $AlFeSiO_2$, and $AlSiO_2$phases, as presented in Fig. 6d, Fig. 6f and Fig. 6h. However, increase in gas flow rate from 7 to 10 L/min at heat input of 52 J (70 A) reduced the presence of SiO_2 as shown in Fig. 7a and Fig. 7b. This trend is noticed with 110 A and 130 A. The presence of SiO_2 significantly reduced with increasing shielding gas flow rate. In addition, increasing shielding gas flow rate refined the segregation of the $AlFeSiO_2$ phase. On the other hand, with increasing heat input (current), the presence of SiO_2 became more significant. This caused fracture of the weld joint instead of parent metals, as presented in Fig. 5b because higher current resulted in higher heat input that promoted prolong solidification, which enhanced spontaneous diffusion of oxygen. It has been reported that high electrical current leads to increased heat input, which in turn promotes longer solidification times. This prolonged solidification can enhance the spontaneous diffusion of oxygen, especially in certain materials or processes like welding. The increased heat input provides more energy for the material to absorb and for oxygen to diffuse, potentially affecting the final microstructure and properties of the material [13]. However, when the gas flow rate is increased, there is a reduction in diffusion of oxygen. Thus, a significant reduction is seen in the SiO2 as shown in Fig. 7b.

3.2. X-ray diffraction analysis

X-ray Diffraction (XRD) analysis is a tool that is often used to identify the phase composition of crystalline substances. It helps to understand the crystallographic texture, crystal orientation and measurement of lattice parameters. Most aluminium alloys experience no allotropic phase transformation since much of the control of microstructure and properties rely on precipitation reactions from α Al into $CuAl_2$ or $CrAl_7$ depending on the solubility level of the alloying elements [14].

The distribution of the phases depends on the heat input and shielding gas flow rate. The presence of SiO_2 within the weld joint primarily indicates the diffusion of oxygen impurity. It has been reported that the presence of SiO_2 (silicon dioxide) in a weld joint is generally a strong indication of the diffusion of oxygen into the weld material, particularly during the high-temperature welding process. The reaction of oxygen with silicon, a common constituent in many weldable metals, forms SiO_2 [15].

3.3. Hardness

Fig. 8 shows the Vickers hardness values of the dissimilar welded samples at different current and gas flow rates. In Fig. 8, there are increased gas flow rates while the input heat (current) applied is kept constant. The hardness profiles along the cross-section of each of the samples are shown. The hardness values of AA6070 are significantly higher than that of AA100 in all tested regions of base metal, heat affected zone, and fusion zone (weld joint). The lower hardness values seen in AA1100 was due to the pure nature of the alloy. AA1100 is a pure aluminium-based alloy (99 % Al), which attained its hardness from intermetallic binary and ternary phases of Al_3Fe and $Al - Fe - Si$ presence. Furthermore, $Al - Fe_4Al_13$ phase is not expected because there was no rapid cooling solidifi-

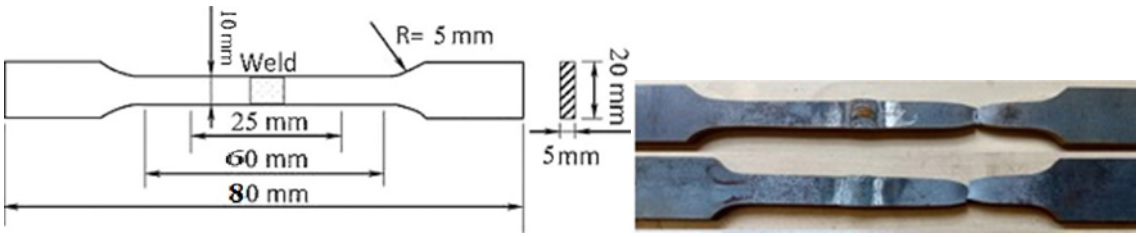

Figure 5: (a) Schematic diagram of the tensile test sample. (b) Typical fractured samples after tensile test [12].

cation process in the base metal [16]. $Al-Fe$ phase is expected to dominate the $Al-Fe-Si$phase because the maximum equilibrium solid solubility of silicon in aluminium is attainable with 1.6 % Si presence in the alloy. However, this did not happen because of the presence of iron as shown in Table 3. During welding process, the heat input was relatively the same with steady increase in gas flow-rate, as presented in Table 4. The AA6070 contains Si, Fe, Mg, Zn, Cu and Mn. Hence, the main strengthening phase in AA6070 is Mg_2Si and relative amount of $FeMn$, $3Si_2Al_15$ and $CuAl_3$. AA6070 also shows some impurity phases such as $AlMnFeSi$, $AlFeSi$ and $AlCrFeSi$, which further promote hardness [17].

The base metal of AA6070, the HAZ near the AA6070 and weld metal show similar high hardness values. The HAZ near AA1100 has the intermediate hardness and base metal of AA1100 was characterised with lowest hardness. The trend of the graphs also indicates that increase in gas flow rate from 7 to 13 L/min resulted in initial increased hardness, which subsequently decreased. At heat input of 52 J (70 A), the average hardness recorded for the base metal of AA6070 when gas flow rates of 7, 10 and 13 L/min were used are 70, 72 and 69 HV respectively. Similarly, for the AA1100, hardness values of 40.9, 49.2 and 39 HV were obtained. This implies that there is a maximum gas flow-rate (10 L/min) for the protection of the weld joint. Beyond this flow-rate, the hardness will be adversely affected causing a decrease in hardness value. Shielding gas serves as a means of protecting molten metals from reacting with atmospheric gases. Optimum protection of the molten metals formed in joints depends on proper selection of shielding gases and the flow-rate. Excessive shielding gas flow-rate may cause turbulence in the gas stream, which may introduce atmospheric contaminants into the weld pool that could result in reduction in hardness. On the other hand, insufficient gas flow-rate would cause weld defects. Thus, there is a need to properly select shielding gas flow-rate.

In the heat-affected zone, there is a fluctuating pattern in the graphs of hardness with increasing gas flow-rate. The hardness values of the HAZ is similar to that of AA6070 base metal with increasing gas flow-rate. However, the HAZ of AA1100 exhibited higher hardness values compared to the base metal, which is independent of gas flow rates. The fusion-zone formed the weld metals, which are components of filler wire (ER4043), AA6070, and AA1100. The hardness values within this region is a function of the combination of welded materials. The weld joint demonstrated the highest hardness value of 72 HV at 70 A and 13 L/min gas flow rate. Welded areas of aluminium alloys are characterised by hardness of brittle intermetallic phases of FeAl3 and Fe2Al5 [18]. The formation of such phases is not pronounced because increase in hardness values was not recorded. The base metal of AA6070 and welded areas have similar hardness values, which suggests that there is a compatibility between the base metal of AA6070 and the filler metal. The gas flow rate is a major parameter that determines the amount of protection attainable to weld joint. It is expected that the higher the gas flow (L/min), the better the protection of the weld joint. Hence, optimum gas flow-rate is imperative to limiting wastage and promotes cost effectiveness.

3.4. Tensile Strength

Table 5 presents the influence of gas flow rates and heat input (current) on the ultimate tensile strength (UTS) of the welded aluminium alloys. At the same heat input (52-53 J/mm), there is an initial increase in UTS of the weld joint when gas flow rate is increased. However, beyond 10 L/min, the UTS reduced significantly with increasing gas flow rate. Furthermore, when there is an increasing heat input, the UTS reduced significantly, except for the 130 A @ 10 L/min. There is an optimum flow rate for the welding process that enhances the UTS.

Fig.9 shows the response of tensile strength to the increase in gas flow rate at the same heat input (current). During the tensile test analysis, some samples mainly fractured from the base metal of AA1100 as it has been established that cracks propagate through the base metal rather than weld joint [12] as shown in Fig. 5b. Other samples fractured in the weld joints. The fracure pattern of joint depends on the weakest region of the sample. Fig. 9a indicates that for heat input of 52 J (70 A) and increasing gas flow rate, there is a similarity in the trend of tensile property. The tensile strain ranged between 25 and 30 %. The fracure pattern is dutile with the AA1100 base metal. At heat input of 66 J (110 A), there is a similar pattern of the tensile property when the gas flow rate was increased except for the 13 L/min that exhibited brittle fracture through the weld metal (Fig. 9b). The tensile strain ranged between 13 and 43 % and the gas flow rate of 10 L/min exhibited the optimum performance. Further brittle fracture was noticed with heat input of 69 J when the gas flow rates were 7 L/min and 13 L/min. The tensile property of weld joint is a function of the weakest point within the alloy. High heat input promotes crack propagation through the weld zone. Thus, brittle fracture occurred irrespect of the flow rates, as noticed in Fig. 9c. However, the highest UTS of 86 MPa was demonstrated at 130 A and 10 L/min of the weld joint.

4. Conclusion

This study has investigated the influence of heat input and shielding gas flow rate on the microstructure and mechanical properties of V-joint welded aluminium alloys of 1100 and 6070 plates. The microstructure revealed the presence of $\alpha-Al$, SiO_2, $AlFeSiO_2$, and $AlSiO_2$ phases in the weld joint (fusion zone), which were influenced by the applied heat input and gas flow rate. At a current of 70 A, and shielding gas flow rate of 7 L/min, the microstructure showed more of dendritic structure, which mainly contained $\alpha-Al$ and $AlSiO_2$. When the gas flow rate increased to 10 L/min, the dendritic structure broke into platelets with no oxygen gas diffusion. The weld joint demonstrated the highest hardness value of 72 HV at 70 A and 13 L/min gas flow rate. The weld joint demonstrated the highest ultimate tensile strength of 86 MPa at 130 A and 10 L/min. The welding current plays a significant role in weld penetration and heat input, affecting the mechanical properties of the weld joint. Using a protective gas like argon or helium,

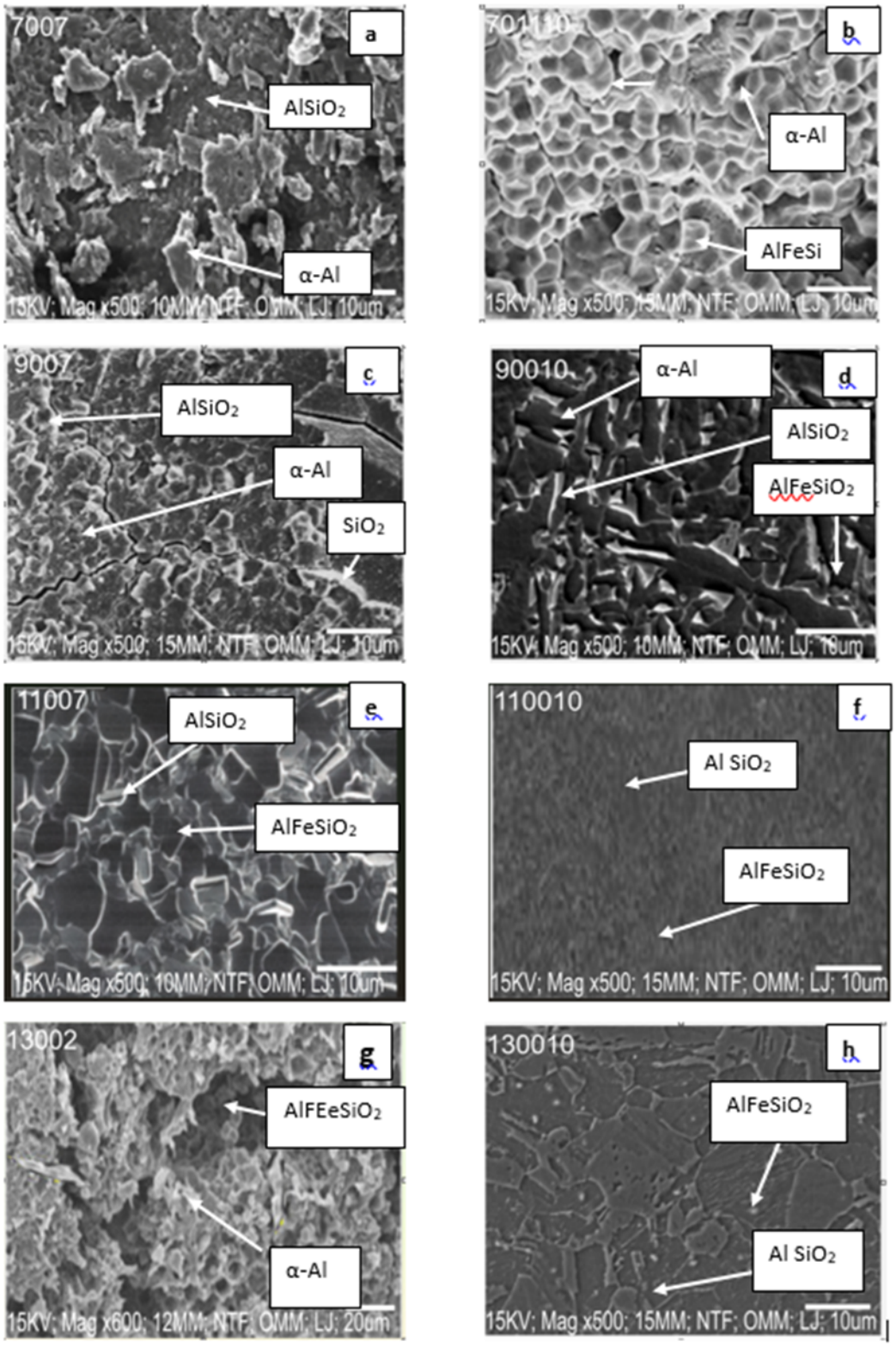

Figure 6: Scanning electron microscope results of samples (a) 70 A @ 7 L/min, (b) 70 A @ 10 L/min, (c) 90 A @ 7 L/min, (d) 90 A @ 10 L/min, (e) 110 A @ 7 L/min, (f) 110 A @ 10 L/min, (g) 130 A @ 7 L/min and (h) 130 A @ 7 L/min.

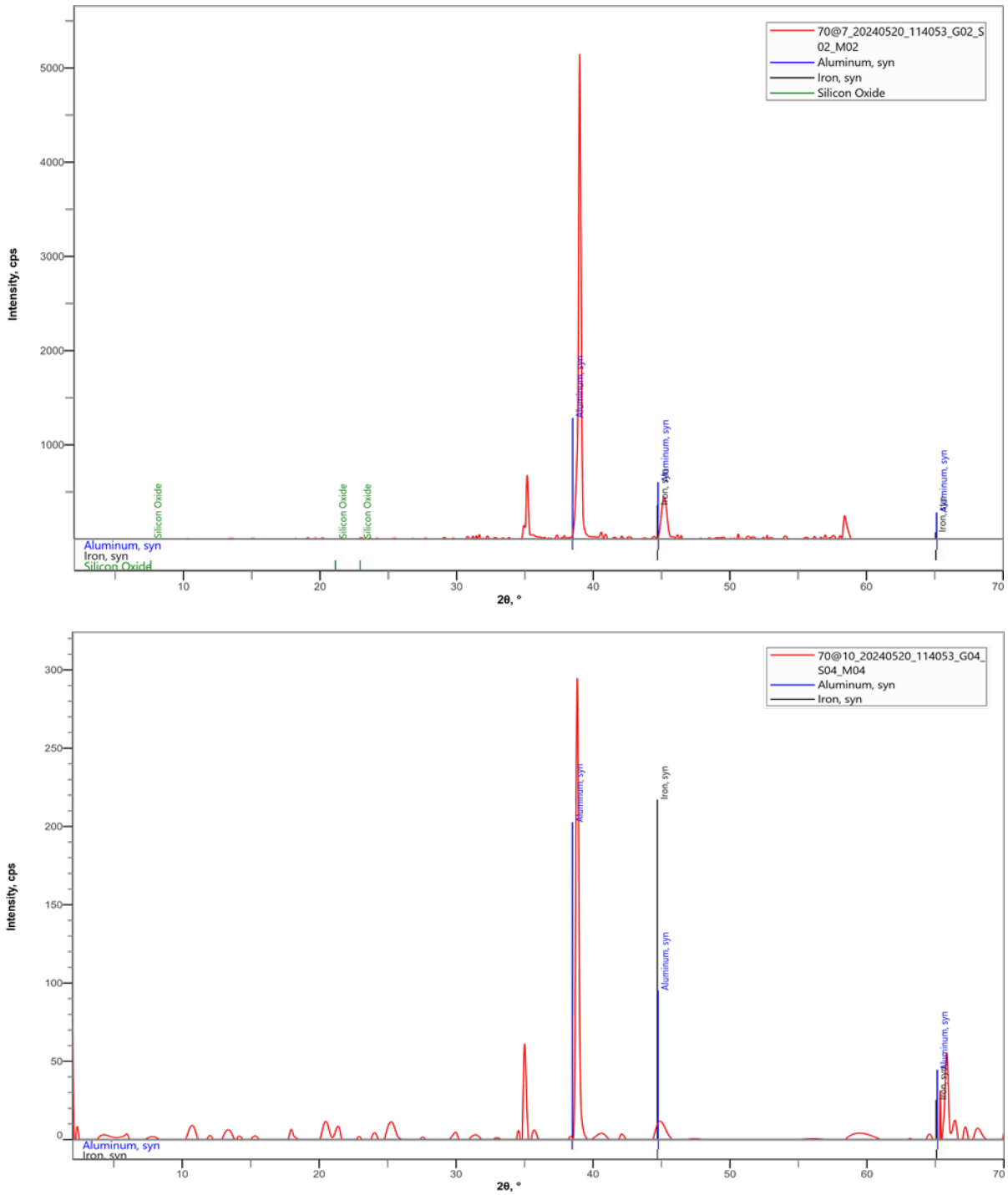

Figure 7: (a) XRD result of sample welded at 70 A and gas rate of 7 L/min. (b) XRD result of sample welded at 70 A and gas rate of 10 L/min .

Table 5: Gas flow rate and heat input (current) and the ultimate tensile strength.

Welding parameters	UTS (MPa)	Welding parameters	UTS (MPa)	Welding parameters	UTS (MPa)	Welding parameters	UTS (MPa)
70 A @ 7 L/min	82.43	90 A @ 7 L/min	62.52	110 A @ 7 L/min	69.15	130 A @ 7 L/min	61.82
70 A @ 10 L/min	67.93	90 A @ 10 L/min	76.66	110 A @ 10 L/min	71.49	130 A @ 10 L/min	86.77
70 A @ 13 L/min	79.79	90 A @ 13 L/min	56.23	110 A @ 13 L/min	47.85	130 A @ 13 L/min	56.92

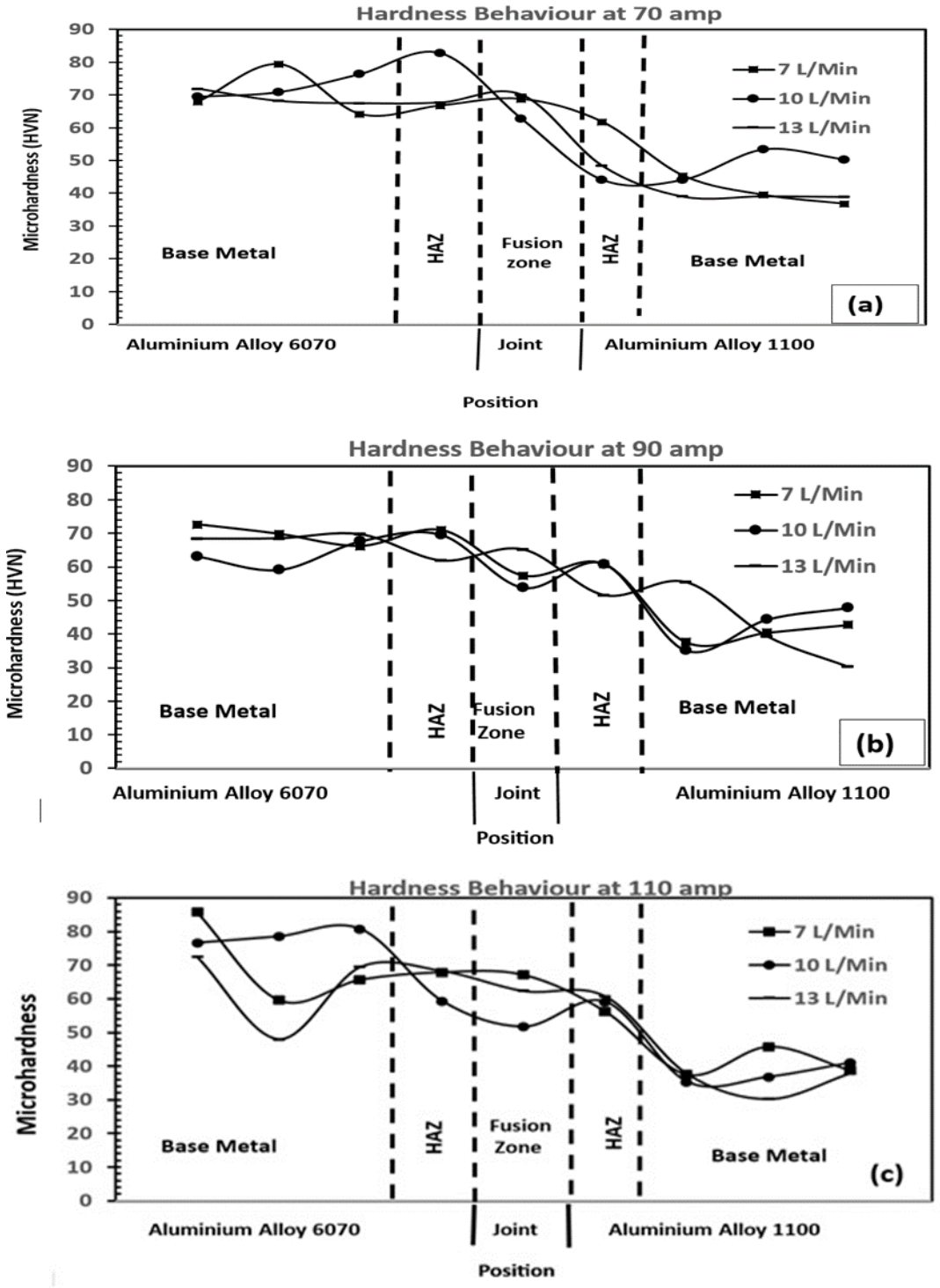

Figure 8: Microhardness profile across the AA6070 and AA1100 dissimilar joints welded at (a) 70 A, (b) 90 A and (c) 110 A.

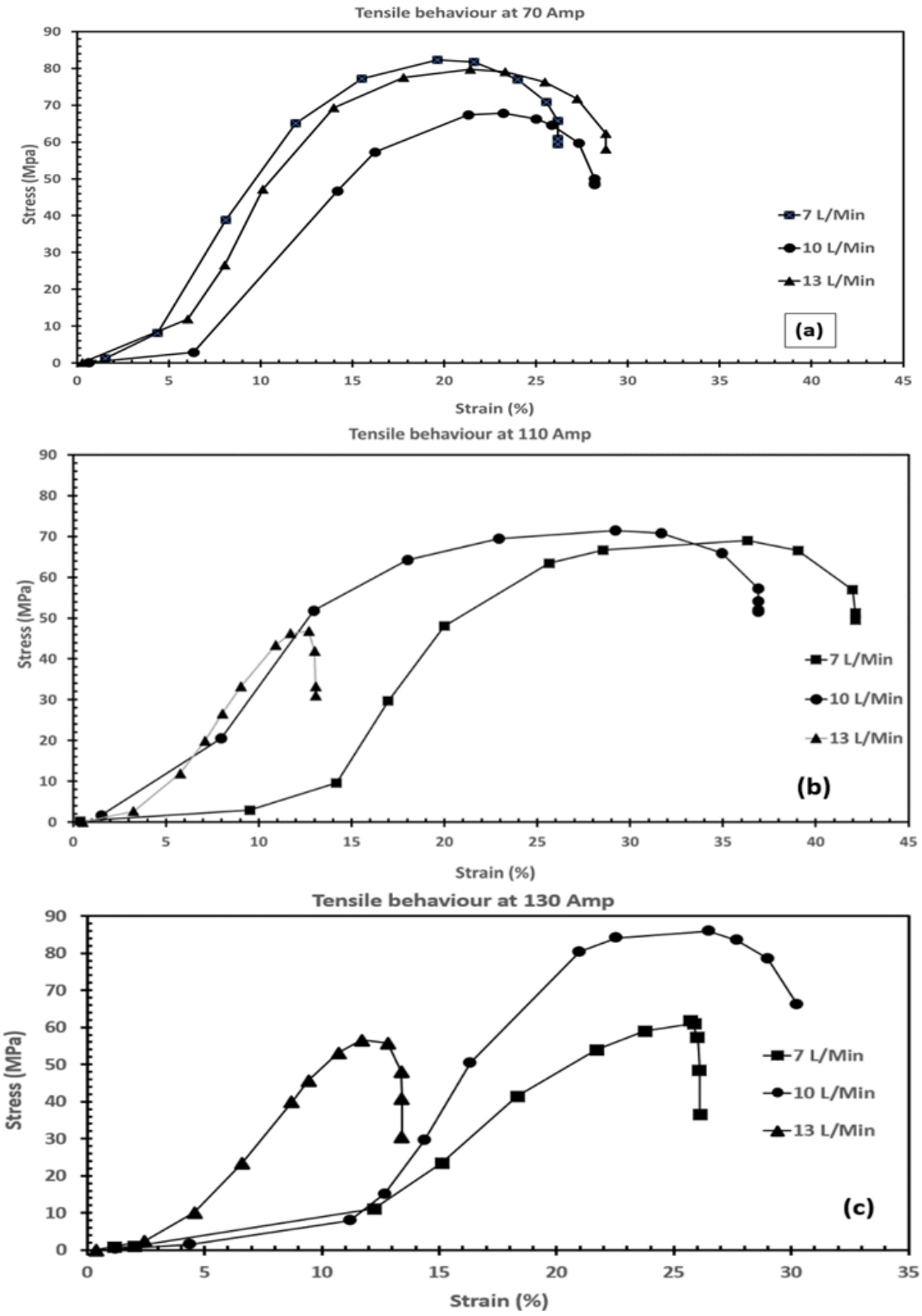

Figure 9: The stress – strain relationship with increasing gas flow rate for (a) 70 A, (b) 110 A and (c) 130 A.

and adjusting the flow rate to ensure adequate shielding without causing excessive turbulence is also important. For some applications, choice or selection of filler metals are needed to achieve desired weld geometry and properties. The choice of filler wire depends on the specific alloy being welded. By carefully considering these factors one can optimize TIG welding parameters for AA1100-AA6070 aluminium alloys to achieve high-quality welds with desirable mechanical properties for the intended applications. Furthermore, maintaining a short arc length to minimize heat input and ensure stable arc performance and adjusting welding speed to ensure proper fusion without overheating the base metal are also important.

References

[1] Torzewski J, Lazinska M, Grzelak K, Szachogłuchowicz I & Mierzynski J, Microstructure and mechanical properties of dissimilar friction stir welded joint AA7020/AA5083 with different joining parameters, *Materials*, 15(5) (2022) 1910. ISSN 1996-1944. https://doi.org/10.3390/ma15051910.

[2] Jannet S, Mathews P & Raja R, Comparative investigation of friction stir welding and fusion welding of 6061 T6 – 5083 O aluminum alloy based on mechanical properties and microstructure, *Bulletin of the Polish Academy of Sciences Technical Sciences*, 62(4) (2014) 791–795. ISSN 2300-1917. https://doi.org/10.2478/bpasts-2014-0086.

[3] Kumar L, Yazar K & Pramanik S, Effect of fusion and friction stir welding techniques on the microstructure, crystallographic texture and mechanical properties of mild steel, *Materials Science and Engineering: A*, 754 (2019) 400–410. ISSN 0921-5093. https://doi.org/10.1016/j.msea.2019.03.100.

[4] Kanemaru S, Sasaki T, Sato T, Mishima H, Tashiro S & Tanaka M, Study for TIG–MIG hybrid welding process, *Welding in the World*, 58(1) (2013) 11–18. ISSN 1878-6669. https://doi.org/10.1007/s40194-013-0090-y.

[5] Jeyaprakash N, Haile A & Arunprasath M, The parameters and equipment used in tig welding: A review, *International Journal of Engineering and Science*, 4(2) (2015) 11–20.

[6] Singh A K, Dey V & Rai R N, Techniques to improve weld penetration in TIG welding (A review), *Materials Today: Proceedings*, 4(2) (2017) 1252–1259. ISSN 2214-7853. https://doi.org/10.1016/j.matpr.2017.01.145.

[7] Madavi K, Jogi B & Lohar G, Metal inert gas (MIG) welding process: A study of effect of welding parameters, *Materials Today: Proceedings*, 51 (2022) 690–698. ISSN 2214-7853. https://doi.org/10.1016/j.matpr.2021.06.206.

[8] Gudala S S, Metta U K & Dangeti M, Experimental analysis on mechanical properties with microstructures on Aluminium alloy 6070 welds with H14 steel, *International Journal for Research in Applied Science and Engineering Technology*, 12(1) (2024) 597–611. ISSN 2321-9653. https://doi.org/10.22214/ijraset.2024.58017.

[9] Habba M I A, Alsaleh N A, Badran T E, El-Sayed Seleman M M, Ataya S, El-Nikhaily A E, Abdul-Latif A & Ahmed M M Z, Comparative study of FSW, MIG, and TIG welding of AA5083-H111 based on the evaluation of welded joints and economic aspect, *Materials*, 16(14) (2023) 5124. ISSN 1996-1944. https://doi.org/10.3390/ma16145124.

[10] Osoba L, Ayoola W, Adegbuji Q & Ajibade O, Influence of heat inputs on weld profiles and mechanical properties of carbon and stainless steel, *Nigerian Journal of Technological Development*, 18(2) (2021) 135–143. ISSN 0189-9546. https://doi.org/10.4314/njtd.v18i2.8.

[11] Ayoola W A, Adeosun S O, Sanni O S & Oyetunji A, Effect of casting mold on mechanical properties of 6063 Aluminum alloy, *Journal of Engineering Science and Technology*, 7(1) (2012) 89–96.

[12] Rakesh M & Kumar T R, Comparative study of different filler materials on Aluminium alloys using TIG welding, *International Journal of Engineering Research and Technology*, 8(8) (2019) 240–244.

[13] David S A, Babu S S & Vitek J M, Welding: Solidification and microstructure, *JOM*, 55(6) (2003) 14–20. ISSN 1543-1851. https://doi.org/10.1007/s11837-003-0134-7.

[14] Jaradeh M M R. *The effect of processing parameters and alloy composition on the microstructure formation and quality of DC cast Aluminium alloys*. Ph.D. thesis, Department of Material Science and Engineering, Mid Sweden University, Sweden (2006).

[15] Binande P, Shahverdi H R & Farnia A, Study on the effect of flux composition on the melting efficiency of A-TIG of aisi 316l stainless steel: Experimental and analytical approaches, *Journal of Materials Research and Technology*, 33 (2024) 9092–9108. https://doi.org/10.2139/ssrn.4994801.

[16] Allen C, O'Reilly K, Cantor B & Evans P, Intermetallic phase selection in 1XXX Al alloys, *Progress in Materials Science*, 43(2) (1998) 89–170. ISSN 0079-6425. https://doi.org/10.1016/s0079-6425(98)00003-6.

[17] Wang H, Sun W & Xing Y, Microstructure analysis on 6061 Aluminum alloy after casting and diffuses annealing process, *Physics Procedia*, 50 (2013) 68–75. ISSN 1875-3892. https://doi.org/10.1016/j.phpro.2013.11.013.

[18] Emamy M, Pourbahari B & Mostafapour M, Significant grain refinement and enhance mechanical properties of 6070 Al alloy via Ti/Sr addition and hot extraction, *Journal of Ultrafine and Nanostructured Materials*, 53(2) (2020) 190–203. https://doi.org/10.22059/jufgnsm.2020.02.11.